JACS
JOURNAL OF THE AMERICAN CHEMICAL SOCIETY
pubs.acs.org/JACS
Article

Attosecond Charge Migration in Molecules Imaged by Combined X-ray and Electron Diffraction

Haiwang Yong,* Shichao Sun, Bing Gu, and Shaul Mukamel*

Cite This: J. Am. Chem. Soc. 2022, 144, 20710−20716
Read Online
ACCESS | Metrics & More | Article Recommendations | Supporting Information

ABSTRACT: We show how ultrafast gas-phase X-ray and electron diffraction signals can be combined to generate real-space movies of charge migration dynamics in molecules. Charge migration denotes short time electronic charge redistribution upon photoexcitation of molecules where the nuclei are frozen. In this regime, we identify a mixed electronic−nuclear interference term that can be cleanly singled out. Using the ground-state nuclear structure as a reference, the phase information in this signal allows its inversion to real space and the capture of electronic charge density movies on the attosecond time scale.

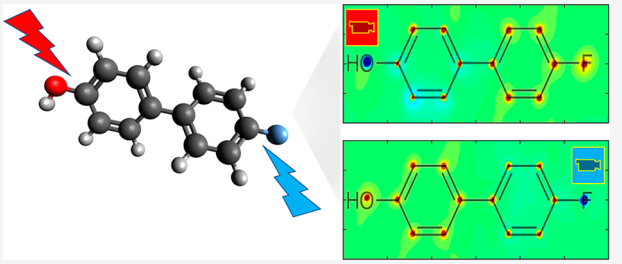

INTRODUCTION

Molecular wave functions are spatially diffuse and spread over many atoms within a molecule exhibiting no motion. The femtosecond time scale is unique for creating superpositions of multiple vibrational wave functions producing the spatially localized wavepacket with coherent nuclear motions. This laid the foundation of the field of femtochemistry.[1] With the rapid developments of attosecond pulses in the 21st century, a coherent superposition of multiple electronic states can be created resulting in coherent electronic motion denoted charge migration.[2−4] This phenomenon has been intensively studied theoretically over the last 20 years,[5−11] leading to the birth of "attochemistry". The goal of attochemistry is to create a new way of doing chemistry by observing and controlling motions of molecular electrons on their intrinsic time scale.[12]

Measurements of charge migration have been broadly reported,[13−20] while the direct real-space imaging of its time-evolving charge density is still challenging. Ultrafast X-ray and electron diffraction techniques hold the promise of real-space tracking of electron motions in molecules.[21,22] Several theoretical studies of probing charge migration by ultrafast X-ray scattering have been reported.[23−25] However, the molecular charge density cannot be directly retrieved from such signals. This is because standard ultrafast gas-phase X-ray diffraction and electron diffraction use homodyne detection which gives the expectation values of products of charge-density operators $\langle \hat{\sigma}^{\dagger}\, \hat{\sigma} \rangle$,[26] rather than the charge density $\langle \hat{\sigma} \rangle$ itself which can be measured by heterodyne detection. Heterodyne-detected diffraction requires an additional reference beam that interferes with the scattered wave.[27−29] X-ray sum-frequency generation diffraction with heterodyne detection could achieve this in molecules;[30,31] its experimental realization is extremely challenging, as it requires two phase-controlled hard X-ray pulses. Self-heterodyne X-ray diffraction has been previously realized in crystalline and powder samples possessing long-range order where the scattering from ground-state molecules is used as a local oscillator to boost the scattering signal from excited-state molecules.[32,33] However, that strategy is not applicable to gas-phase molecules dominated by the single-molecule scattering signal.[34] Similarly, real-space motions of the molecular crystal have been determined from femtosecond electron diffraction data analysis with a known initial ground-state structure.[35] To solve the well-known phase problem for retrieving a quantum molecular movie from diffraction data, the theory of quantum state tomography has been introduced to analyze experimental electron diffraction data.[36,37]

In this theoretical study, we introduce a novel technique for isolating mixed electronic−nuclear interference in electron diffraction (MENIED) for the direct real-space imaging of charge migration in gas-phase molecules by combining two (X-ray and electron) homodyne diffraction measurements (Figure 1). Previously, we have shown how to image the purely nuclear charge density by combining heterodyne-detected X-ray and electron diffraction.[38] The proposed experimental scheme in Figure 1 is much easier to implement, as heterodyne detections are not required in this study. We show that, when subtracting the ultrafast X-ray and electron homodyne diffraction signals, the time-dependence of the signal only comes from a mixed nuclear−electronic term $\sigma^{E}\sigma^{N}$ where $\sigma^{E/N}$ is the electronic/

Received: July 28, 2022
Published: November 1, 2022

https://doi.org/10.1021/jacs.2c07997
J. Am. Chem. Soc. 2022, 144, 20710−20716

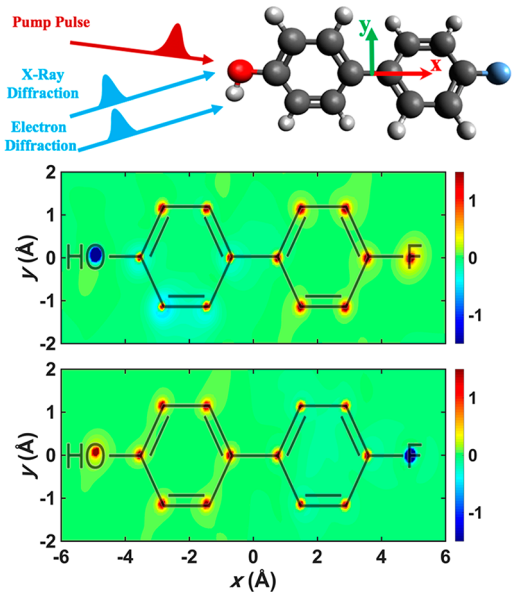

Figure 1. (top) Schematic of proposed experiment and molecular structure of 4-fluoro-4′-hydroxybiphenyl. We assume an oriented molecule located in the x−y plane. Difference electronic charge densities in real space, $\Delta\sigma^{E}_{tot}(\mathbf{r}, t) = \sigma^{E}_{tot}(\mathbf{r}, t) - \sigma^{E}_{0}(\mathbf{r})$, at 0.6 fs after excitation with X-ray pump pulse tuned to oxygen (middle) and fluorine (bottom) K-edges. The charge densities are presented in the x−y plane by integrating over z.

nuclear charge density of the molecule. Because the nuclei of the molecule are frozen during the attosecond charge migration dynamics, the resulting time-dependent diffraction signal constitutes an interference between the time-evolving electronic charge density σ^{E} and the ground-state nuclear structure σ^{N} that serves as a reference local oscillator. The time-evolving electronic charge density of the molecule can thus be directly measured via the proposed technique.

THEORY OF MIXED ELECTRONIC−NUCLEAR INTERFERENCE IN ELECTRON DIFFRACTION

The time-dependent molecular many-electron wave function prepared by a resonant X-ray excitation with a broadband attosecond pulse can be expanded as

$$|\psi(t)\rangle = \sum_i c_i(t)|\varphi_i\rangle \tag{1}$$

where i labels the adiabatic electronic state $|\varphi_i\rangle$ at the equilibrium geometry, $c_i(t)$ is the electronic state amplitude, and t is the time. Equation 1 assumes purely electronic dynamics and neglects nuclear motions, which is justified for the charge-migration time scales that are shorter than the typical nuclear vibrational period of molecules (a few femtoseconds).

Using eq 1, the time-evolving electronic charge density in real space is given by

$$\sigma^{E}_{tot}(\mathbf{r}, t) = \langle\hat{\sigma}^{E}(\mathbf{r}, t)\rangle = \sum_i \rho_{ii}\sigma^{E}_{ii}(\mathbf{r}) + \sum_{i\neq j}\rho_{ji}(t)\,\sigma^{E}_{ij}(\mathbf{r}) \tag{2}$$

where $\mathbf{r}$ is the spatial coordinate, $\sigma^{E}_{ii}(\mathbf{r})$ is the charge density of electronic state i, $\sigma^{E}_{ij}(\mathbf{r})$ is the electronic transition charge density between electronic state i and j, $\rho_{ii} = c_i^* c_i$ represents the electronic population which is stationary after the pump pulse is over while $\rho_{ji}(t) = c_i^* c_j$ is electronic coherence which oscillates with a period inversely proportional to the energy difference between electronic states i and j.

The time-resolved single-molecule (gas-phase) homodyne diffraction signal is written as[26,39]

$$S(\mathbf{q}, T) \propto \int \mathrm{d}t\,|E_p(t - T)|^2 \tilde{S}(\mathbf{q}, t, \omega) \tag{3}$$

where $E_p(t - T)$ is the X-ray/electron probe pulse envelope at delay time T, $\mathbf{q}$ is the scattering momentum transfer, and $\tilde{S}(\mathbf{q}, t, \omega)$ is related to the time-dependent molecular charge density in momentum space.

For X-ray diffraction, $\tilde{S}(\mathbf{q}, t, \omega)$ is given by

$$\tilde{S}^{XRD}(\mathbf{q}, t, \omega) = \sum_{ijk} W_{kji}(\Delta\omega)\,\rho_{ji}(t)\,\sigma^{E}_{ik}(-\mathbf{q})\,\sigma^{E}_{kj}(\mathbf{q}) \tag{4}$$

Here, $\sigma^{E}_{ik}(\mathbf{q})$ is the Fourier transform of the electronic charge-density matrix element between electronic states i and k, and $W_{kji}(\Delta\omega)$ is a window function for a frequency detection window $\Delta\omega$ given by[40,41]

$$W_{kji}(\Delta\omega) = \int_{\omega_p-\Delta\omega}^{\omega_p+\Delta\omega}\int_{-\infty}^{+\infty} C(\delta)\mathrm{e}^{-\mathrm{i}(\omega_s-\omega_p+\omega_{kji})\delta}\mathrm{d}\delta\,\mathrm{d}\omega_s \tag{5}$$

where $C(\delta) = \exp\left[-2\ln 2\frac{\delta^2}{\tau_p^2}\right]$ is a function of the probe pulse duration τ_p, $\omega_{s/p}$ is the angular frequencies of the incident/scattered waves, and $\omega_{kji} = \omega_k - \frac{\omega_j + \omega_i}{2}$ is the angular frequency corresponding to the transition energies of the molecule involving states i, j, and k.

Similarly, for electron diffraction, $\tilde{S}(\mathbf{q}, t, \omega)$ is written as

$$\begin{aligned}\tilde{S}^{UED}(\mathbf{q}, t, \omega) = \frac{1}{q^4}\Bigg\{&\sum_{ijk} W_{kji}(\Delta\omega)\,\rho_{ji}(t)\,\sigma^{E}_{ik}(-\mathbf{q})\,\sigma^{E}_{kj}(\mathbf{q}) \\ &+ W_0(\Delta\omega)\sum_i \rho_{ii}\sigma^{N}_{ii}(-\mathbf{q})\,\sigma^{N}_{ii}(\mathbf{q}) \\ &+ 2\mathcal{R}\Bigg[W_0(\Delta\omega)\sum_i \rho_{ii}\sigma^{E}_{ii}(-\mathbf{q})\,\sigma^{N}_{ii}(\mathbf{q}) \\ &+ \sum_{i\neq j} W_{ji}(\Delta\omega)\,\rho_{ji}(t)\,\sigma^{E}_{ij}(-\mathbf{q})\,\sigma^{N}_{jj}(\mathbf{q})\Bigg]\Bigg\} \\ = \frac{1}{q^4}&(\tilde{S}^{elec}(\mathbf{q}, t, \omega) + \tilde{S}^{nucl}(\mathbf{q}, \omega) + \tilde{S}^{mixed}(\mathbf{q}, t, \omega))\end{aligned} \tag{6}$$

Here, $\tilde{S}^{elec}(\mathbf{q}, t, \omega) = \tilde{S}^{XRD}(\mathbf{q}, t, \omega)$, and $W_0(\Delta\omega)$ represents the window function when $\omega_{kji} = 0$ in eq 5.

By subtracting the two measurements, we obtain S_{diff} as

$$\begin{aligned}S_{diff}(\mathbf{q}, t, \omega) &= \eta\tilde{S}^{UED}(\mathbf{q}, t, \omega) - \tilde{S}^{XRD}(\mathbf{q}, t, \omega) \\ &= \tilde{S}^{nucl}(\mathbf{q}, \omega) + \tilde{S}^{mixed}(\mathbf{q}, t, \omega)\end{aligned} \tag{7}$$

where η is a normalization factor accounting for the Thomson and Rutherford cross sections.[42] Careful normalization of the signal for both measurements is a nontrivial task but is crucial for the proper subtraction of X-ray and electron diffraction signals in order to obtain S_{diff}. Experimental conditions such as the different scattering background and detector response for X-rays and electrons need to be taken into account. Besides, the diffraction signals should be deconvoluted with their respective instrument functions before subtraction to account

https://doi.org/10.1021/jacs.2c07997
J. Am. Chem. Soc. 2022, 144, 20710−20716

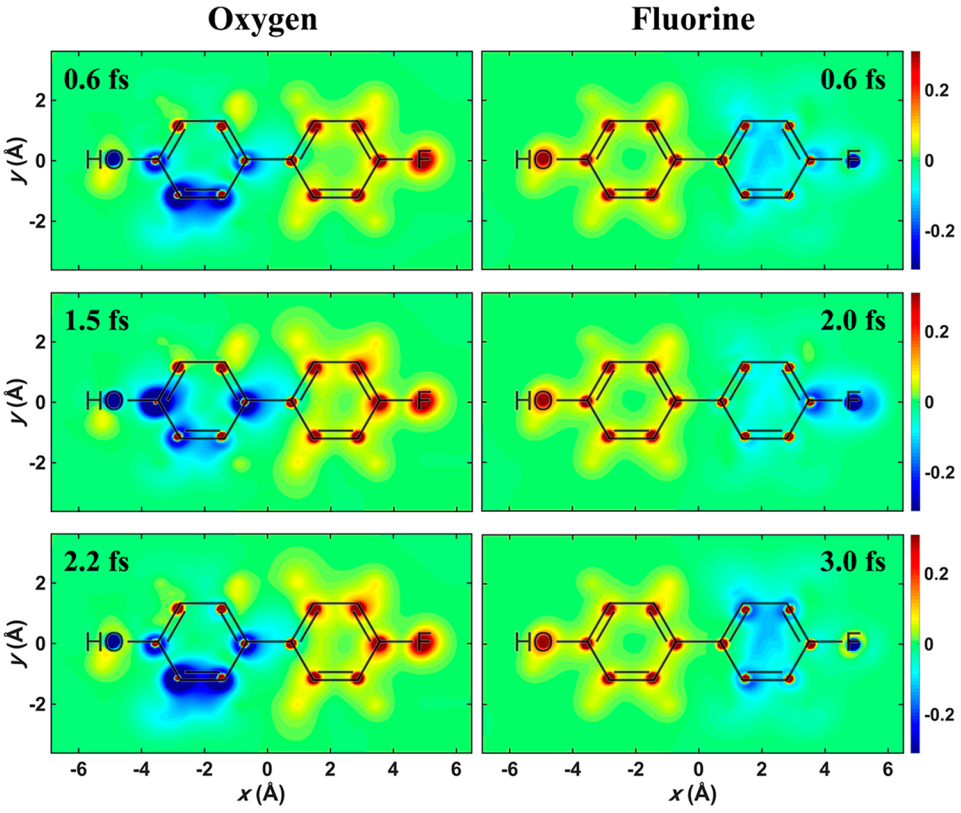

Figure 2. Snapshots of difference electronic charge density, $\Delta\sigma^{E}_{tot}(\mathbf{r}, t)$, in real space for the X-ray pump pulse tuned to the oxygen K-edge (left) and fluorine K-edge (right). The Cartesian coordinates are the same as in Figure 1. The charge densities are presented in the $x-y$ plane by integrating over z.

for the small temporal difference of the X-ray and electron pulse lengths. In this study, we assume a 200 as (sigma) pulse length for both X-ray and electron probe pulses. This is possible through the ongoing developments of both attosecond hard X-ray[43,44] and attosecond relativistic megaelectronvolt electron pulses.[45−47]

In attosecond electron dynamics where nuclear motions can be neglected, $\sigma^{N}(\mathbf{q})$ is constant before and after the excitation, and $\tilde{S}^{mixed}(\mathbf{q}, t, \omega)$ can then be written as

$$\tilde{S}^{mixed}(\mathbf{q}, t, \omega) = 2\mathcal{R}\left[\left(W_0(\Delta\omega)\sum_i \rho_{ii}\sigma^{E}_{ii}(-\mathbf{q}) + \sum_{i\neq j} W_{ji}(\Delta\omega)\,\rho_{ji}(t)\,\sigma^{E}_{ij}(-\mathbf{q})\right)\sigma^{N}(\mathbf{q})\right] \quad (8)$$

The purely nuclear term $\tilde{S}^{nucl}(\mathbf{q}, \omega)$ is time-independent and cancels out in the time-dependent difference signal $\Delta S_{diff}(\mathbf{q}, t, \omega) = S_{diff}(\mathbf{q}, t, \omega) - S_{diff}(\mathbf{q}, t < 0, \omega) = \tilde{S}^{mixed}(\mathbf{q}, t, \omega) - \tilde{S}^{mixed}(\mathbf{q}, t < 0, \omega)$. Here, $S_{diff}(\mathbf{q}, t < 0, \omega)$ represents the signal before the presence of the pump pulse.

If the detection window is much broader than the relevant electronic transition energies of the system, then all inelastic transitions are detected with equal weight, and the window function is independent of the angular frequency ω_{ji}. $\tilde{S}^{mixed}(\mathbf{q}, t)$ in eq 8 can be simplified as

$$\tilde{S}^{mixed}(\mathbf{q}, t) = W_0(\Delta\omega)2\mathcal{R}[\sigma^{E}_{tot}(-\mathbf{q}, t)\,\sigma^{N}(\mathbf{q})] \quad (9)$$

where $W_0(\Delta\omega)$ is solely a function of the instrument and is independent of molecular response. The time-dependent difference signal ΔS_{diff} becomes

$$\Delta S_{diff}(\mathbf{q}, t) = W_0(\Delta\omega)2\mathcal{R}[\Delta\sigma^{E}_{tot}(-\mathbf{q}, t)\,\sigma^{N}(\mathbf{q})] \quad (10)$$

where $\Delta\sigma^{E}_{tot}(\mathbf{q}, t) = \sigma^{E}_{tot}(\mathbf{q}, t) - \sigma^{E}_{0}(\mathbf{q})$ is difference electronic charge density in $\mathbf{q}$-space. Here, $\sigma^{E}_{0}(\mathbf{q})$ represents the total electronic charge density prior to the pump pulse, i.e., $\sigma^{E}_{tot}(\mathbf{q}, t < 0) = \sigma^{E}_{0}(\mathbf{q})$. The $\sigma^{N}(\mathbf{q})$ can be obtained from ground-state nuclear geometry. $\Delta S_{diff}(\mathbf{q}, t)$ thus directly measures the time-evolving electronic charge density, thus providing movies of charge migration dynamics in molecules. Whether the diffraction signal is solely related to the total time-dependent charge density of the molecule, i.e., $\langle\hat{\sigma}(\mathbf{r}, t)\rangle$, or requires additional molecular information is an interesting issue. Consider wavevector resolution without frequency resolution, which corresponds to a broad detection window $\Delta\omega$. In that case, both single-molecule (gas-phase) heterodyne $\langle\hat{\sigma}(\mathbf{q}, t)\rangle$ and two-molecule (ordered sample) homodyne diffraction $|\langle\hat{\sigma}(\mathbf{q}, t)\rangle|^2$ signals depend solely on the total charge density irrespective of whether the diffraction is elastic or inelastic. In contrast, the single-molecule homodyne diffraction $\langle\hat{\sigma}^{\dagger}(\mathbf{q}, t)\,\hat{\sigma}(\mathbf{q}, t)\rangle$ signal requires the charge-density matrix $\sigma_{ij}(\mathbf{r})$ that goes beyond the expectation value of the charge density and depends on the spectrum of excited states. Once adding frequency resolution with a finite detection window, the total charge density $\langle\hat{\sigma}(\mathbf{r}, t)\rangle$ alone is not enough for obtaining the diffraction signals.

https://doi.org/10.1021/jacs.2c07997
J. Am. Chem. Soc. 2022, 144, 20710−20716

RESULTS AND DISCUSSION

We have applied the MENIED to image the attosecond charge migration of 4-fluoro-4′-hydroxybiphenyl (Figure 1). Fluorinated biphenyls are important building blocks for many devices including liquid crystal displays,[48] organic light emitting diodes,[49] and organic semiconductors.[50] Understanding the interactions between light and push−pull chromophores is fundamental for many practical applications such as in optoelectronics and bioimaging.[51,52] In the present study, the oriented molecule is initially prepared in a coherent superposition of multiple core-excited states by a broadband soft X-ray pulse (fwhm 5 eV) resonant with the oxygen or the fluorine K-edges. Core-excited electronic states are important for understanding many fundamental phenomena such as X-ray radiation damage of human bodies. We have simulated the electron dynamics after X-ray excitation by exactly solving the time-dependent Schrödinger equation (see full details in the SI). An attosecond X-ray pump pulse, 0.365 fs (fwhm), is explicitly included in the electron dynamics simulation. We focus on the charge migration dynamics originating from electronic coherence of core-excited states after the pump pulse is over (at $t \geq 0.6$ fs). The sub-5 fs dynamics is simulated which is comparable with the lifetime of oxygen and fluorine core-excited states. The subsequent Auger−Meitner effect could cause the decay of core-excited states resulting in electronic dephasing. The Auger−Meitner process is the dominant mechanism for relaxation following X-ray absorption in most biologically relevant molecules. Its time-dependent electron yield has been used as an indirect indicator to probe the evolution of a coherent core-hole excitation in nitric oxide in a recent study.[53] The population dynamics during the pump pulse is shown in the SI. The resonant X-ray excitation creates a localized "hole" (negative intensities, blue) near the excited core region and a delocalized valence "electron" (positive intensities, red) across the entire molecule right after the pump pulse is over, as shown in the middle and bottom panels of Figure 1. The key core-excited states with their molecular orbital excitation contributions involved in the simulated electron dynamics are summarized in the SI (see Table S2 and Figure S3). The resulting charge migration dynamics triggered by oxygen and fluorine core excitations are clearly distinct. MENIED is then used for imaging the electron dynamics at various delay times after core excitation. X-ray and electron diffraction can be performed separately as long as the chemical environment of the measured sample is maintained. The signals of MENIED are obtained by subtracting these two diffraction signals with careful normalization.

Snapshots of the electron dynamics for the oxygen and fluorine excitation are shown in Figure 2 (full electronic dynamics are given in the SI as video files). Figure 2 (top) shows the same difference electronic charge density at 0.6 fs as in Figure 1 but with a smaller color intensity scale, so that subtle details can be more visible. For the oxygen K-edge excitation at 0.6 fs, a weaker delocalized negative density "hole" created around the left benzene ring manifests in Figure 2 in addition to the dominant negative density "hole" created around the oxygen atom. Similarly, for the fluorine K-edge excitation at 0.6 fs, a weaker delocalized negative density "hole" around the right benzene ring becomes visible in addition to the localized "hole" near the fluorine atom. This corresponds to the relaxation of occupied molecular orbitals due to the generation of a 1 s hole upon X-ray excitation. Snapshots at different delay times (see Figure 2 and videos in the SI) reveal that fast charge oscillation dynamics within one benzene ring can be seen in both cases. For the oxygen core excitation, electron density oscillates between two lower carbon atoms and two middle carbon atoms of the left benzene ring with a ∼1.6 fs period, while for the fluorine excitation, the charge oscillation appears within the right benzene ring with a period of ∼2.4 fs. Interestingly, there is a weak long-distance electronic motion following the oxygen excitation where electrons slowly migrate from the left ring to the right ring. This is shown by the gradually larger positive intensities around the right ring at 1.5 and 2.2 fs compared to 0.6 fs. This long-distance electron dynamics between two benzene rings is however not visible for the fluorine excitation case. This could be due to the fact that the hydroxyl group (−OH) is an electron-donating group with a strong activating strength, while the fluoro group is an electron-withdrawing group with very weak deactivating strength.

The electron dynamics in Figure 2 is well captured by the MENIED simulated in Figure 3 (full simulated signals are given in the SI as video files). Diffraction patterns in Figure 3 show clear interfering beating features that are characteristic in heterodyne diffraction signals,[30,38] demonstrating the self-heterodyne nature of the $\Delta S_{\text{diff}}(\mathbf{q}, t)$ signal in eq 10. This can be interpreted as heterodyne detection of the electronic charge density where the nuclear structure serves as a local reference. The regions where the signal changes the most are marked by the black circles in Figure 3. The MENIED results for oxygen K-edge excitation and fluorine K-edge excitation are clearly distinct, showing the signal's ability to image the charge

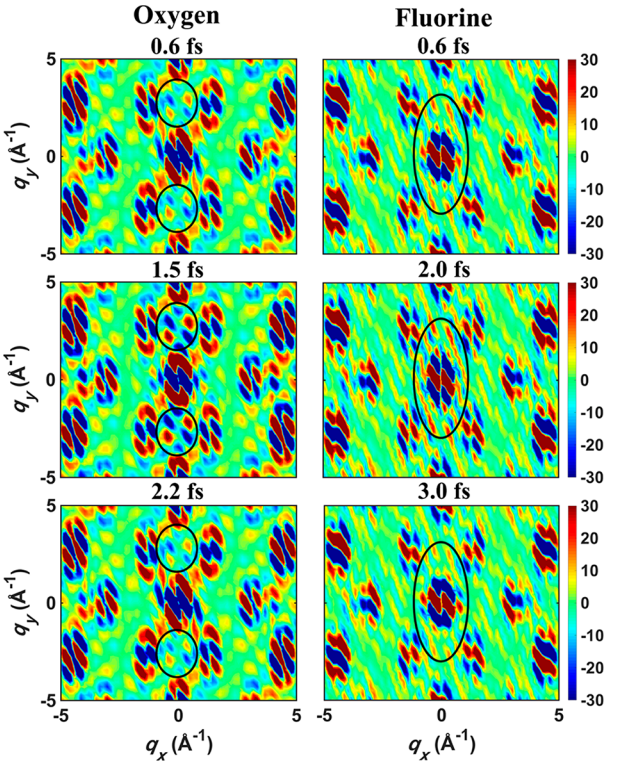

Figure 3. Snapshots of time-dependent difference signal, $\Delta S_{\text{diff}}(\mathbf{q}, t)$ in eq 10, for the X-ray pump pulse tuned to the oxygen K-edge (left) and fluorine K-edge (right). The Cartesian coordinates are the same as in Figure 1. The signals are shown in the q_x−q_y plane ($q_z = 0$).

https://doi.org/10.1021/jacs.2c07997
J. Am. Chem. Soc. 2022, 144, 20710−20716

migration dynamics. The signal in Figure 3 originates from $\Delta\sigma^{E}_{tot}(\mathbf{q}, t)$ $\sigma^{N}(\mathbf{q})$ rather than the time-evolving electronic charge density $\Delta\sigma^{E}_{tot}(\mathbf{q}, t)$. A reconstruction process is needed to obtain the electronic charge density. This can be achieved by calculating $\sigma^{N}(\mathbf{q})$ from the ground-state nuclear geometry of the molecule. As illustrated in Figure 4, the modified diffraction signal is almost identical to the Fourier-transformed electronic charge density. This allows the inversion of the signal from momentum space to the real-space electronic charge density, generating the charge migration movies seen in Figure 2.

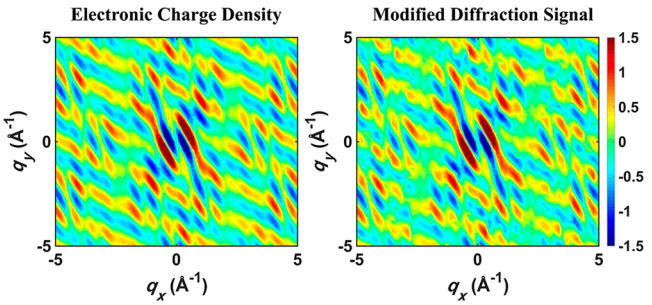

Figure 4. Real part of difference electronic charge density in **q**-space $\mathcal{R}[\Delta\sigma^{E}_{tot}(\mathbf{q}, t)]$ (left) and modified diffraction signal constructed by $\mathcal{R}\left[\frac{\Delta S_{diff}(\mathbf{q}, t)}{\sigma^{N}(\mathbf{q})}\right]$ (right). Both electronic charge density and signal are shown in the q_x−q_y plane (q_z = 0). The results from the oxygen excitation at 2.2 fs are used for demonstration.

CONCLUSIONS

In this study, we have simulated the signal for an oriented molecule, while the idea is equally applicable to a sample of randomly oriented molecules. Measuring the oriented sample allows the direct retrieval of full-dimensional electronic charge densities rather than the one-dimensional radial distribution function obtained from an isotropic sample. Both X-ray diffraction and electron diffraction from three-dimensionally aligned gas-phase molecules have been demonstrated experimentally.[54,55] Since the charge migration dynamics happens in ultrafast time scales which are much shorter compared to the rotational motion of the molecule, the time window of the optimal degree of alignment is long enough for studying attosecond electron dynamics. We note that, in order to generate the charge migration movies shown in Figure 2, a high degree of alignment is required, and the angular spread of the molecules with imperfect alignment needs to be taken into account in the reconstruction procedure.

To estimate the required signal-to-noise ratio for resolving the desired difference signal in Figure 3, we have simulated the time-dependent diffraction signals measured independently with electron (ΔS_{UED}) and X-ray (ΔS_{XRD}) diffraction (see Figure S4 in the SI) which show the same order of magnitude compared to their difference signal (ΔS_{diff}). Because the magnitude of the diffraction signal is proportional to the square of the number of electrons in the molecule, and the desired signal mainly comes from a single electron, the change of signal is about $1 - \frac{97^2}{98^2} = 2\%$ for a molecule with 98 electrons. This corresponds to a ∼0.9% change of the signal for oxygen K-edge excitation (45% excitation fraction) and a ∼0.7% change for fluorine K-edge excitation (36% excitation fraction) simulated in this study. This is within the current experimental detection limit of time-resolved gas-phase X-ray and electron diffraction techniques.[56,57] The key instrumental challenge for the proposed experiment is the attosecond temporal resolution required for both X-ray and electron diffraction. These could become feasible in the near future with the rapid development of XFELs[43,44] and relativistic megaelectronvolt electron beams.[46,47]

In summary, in this theoretical study, we have shown that the attosecond charge migration in gas-phase molecules can be directly imaged by combining ultrafast X-ray and electron homodyne diffraction. We demonstrated that, when subtracting two standard (homodyne) diffraction signals, the time-dependence of the signal only comes from a mixed nuclear−electronic interference term in electron diffraction. This is different from our previous study where we proposed to image the purely nuclear charge density by combining heterodyne-detected ultrafast X-ray and electron diffraction.[38] The pump excitation requires a tunable broadband attosecond soft X-ray pulse with a pulse intensity in the linear regime, which can be achieved with table-top high-harmonic generation X-ray sources.[58−60] Attosecond hard X-ray and electron pulses are required for monitoring charge migration dynamics. Here, we propose to use the MENIED to monitor the coherent core-hole excitation in molecules. Since the method works for any attosecond electron dynamics where the nuclei are frozen, charge migration dynamics of valence electrons initiated by other excitation processes such as strong-field ionization[10] or stimulated X-ray Raman[23,61] can also be studied by the proposed scheme.

ASSOCIATED CONTENT

Supporting Information

The Supporting Information is available free of charge at https://pubs.acs.org/doi/10.1021/jacs.2c07997.

Ab initio quantum chemistry and electron dynamics simulations (PDF)

Video S1: Difference electronic charge density in real space and the MENIED for the X-ray pump pulse tuned to the oxygen K-edge (AVI)

Video S2: difference electronic charge density in real space and the MENIED for the X-ray pump pulse tuned to the fluorine K-edge (AVI)

AUTHOR INFORMATION

Corresponding Authors

Haiwang Yong − *Department of Chemistry, University of California, Irvine, California 92697, United States; Department of Physics and Astronomy, University of California, Irvine, California 92697, United States;* orcid.org/0000-0002-5860-4259; Email: h.yong@uci.edu

Shaul Mukamel − *Department of Chemistry, University of California, Irvine, California 92697, United States; Department of Physics and Astronomy, University of California, Irvine, California 92697, United States;* orcid.org/0000-0002-6015-3135; Email: smukamel@uci.edu

Authors

Shichao Sun − *Department of Chemistry, University of California, Irvine, California 92697, United States;*

Department of Physics and Astronomy, University of California, Irvine, California 92697, United States; orcid.org/0000-0002-7680-3972

Bing Gu − *Department of Chemistry, University of California, Irvine, California 92697, United States; Department of Physics and Astronomy, University of California, Irvine, California 92697, United States;* orcid.org/0000-0002-5787-3334

Complete contact information is available at: https://pubs.acs.org/10.1021/jacs.2c07997

Notes

The authors declare no competing financial interest.

■ ACKNOWLEDGMENTS

The work was primarily supported by the Chemical Sciences, Geosciences, and Biosciences Division, Office of Basic Energy Sciences, Office of Science, U.S. Department of Energy through Award DE-FG02-04ER15571 (H.Y., S.S., and B.G.). The support of the National Science Foundation (Grant No. CHE-1953045) is gratefully acknowledged (S.M.). S.M. is a fellow of the Hagler Institute for Advanced Study at Texas A&M University.

■ REFERENCES

(1) Zewail, A. H. Femtochemistry: Atomic-scale dynamics of the chemical bond. *J. Phys. Chem. A* **2000**, *104*, 5660−5694.
(2) Kling, M. F.; Vrakking, M. J. J. Attosecond electron dynamics. *Annu. Rev. Phys. Chem.* **2008**, *59*, 463−492.
(3) Nisoli, M.; Decleva, P.; Calegari, F.; Palacios, A.; Martín, F. Attosecond electron dynamics in molecules. *Chem. Rev.* **2017**, *117*, 10760−10825.
(4) Wörner, H. J.; et al. Charge migration and charge transfer in molecular systems. *Struct. Dyn.* **2017**, *4*, 061508.
(5) Cederbaum, L. S.; Zobeley, J. Ultrafast charge migration by electron correlation. *Chem. Phys. Lett.* **1999**, *307*, 205−210.
(6) Kuleff, A. I.; Breidbach, J.; Cederbaum, L. S. Multielectron wave-packet propagation: General theory and application. *J. Chem. Phys.* **2005**, *123*, 044111.
(7) Jenkins, A. J.; Vacher, M.; Twidale, R. M.; Bearpark, M. J.; Robb, M. A. Charge migration in polycyclic norbornadiene cations: Wining the race against decoherence. *J. Chem. Phys.* **2016**, *145*, 164103.
(8) Mauger, F.; et al. Signature of charge migration in modulations of double ionization. *Phys. Rev. A* **2018**, *97*, 043407.
(9) Golubev, N. V.; Vaníček, J.; Kuleff, A. I. Core-valence attosecond transient absorption spectroscopy of polyatomic molecules. *Phys. Rev. Lett.* **2021**, *127*, 123001.
(10) Folorunso, A. S.; et al. Molecular modes of attosecond charge migration. *Phys. Rev. Lett.* **2021**, *126*, 133002.
(11) Kobayashi, Y.; Neumark, D. M.; Leone, S. R. Theoretical analysis of the role of complex transition dipole phase in XUV transient-absorption probing of charge migration. *Opt. Express* **2022**, *30*, 5673−5682.
(12) Merritt, I. C. D.; Jacquemin, D.; Vacher, M. Attochemistry: Is controlling electrons the future of photochemistry? *J. Phys. Chem. Lett.* **2021**, *12*, 8404−8415.
(13) Goulielmakis, E.; et al. Real-time observation of valence electron motion. *Nature* **2010**, *466*, 739−743.
(14) Calegari, F.; et al. Ultrafast electron dynamics in phenylalanine initiated by attosecond pulses. *Science* **2014**, *346*, 336−339.
(15) Kraus, P. M.; et al. Measurement and laser control of attosecond charge migration in ionized iodoacetylene. *Science* **2015**, *350*, 790−795.
(16) Lara-Astiaso, M.; et al. Attosecond pump-probe spectroscopy of charge dynamics in tryptophan. *J. Phys. Chem. Lett.* **2018**, *9*, 4570−4577.
(17) Månsson, E. P.; et al. Real-time observation of a correlation-driven sub 3 fs charge migration in ionized adenine. *Commun. Chem.* **2021**, *4*, 73.
(18) Barillot, T.; et al. Correlation-driven transient hole dynamics resolved in space and time in the isopropanol molecule. *Phys. Rev. X* **2021**, *11*, 031048.
(19) Huang, Y.; et al. Ultrafast hole deformation revealed by molecular attosecond interferometry. *Ultrafast Science* **2021**, *2021*, 9837107.
(20) Schwickert, D.; et al. Electronic quantum coherence in glycine molecules probed with ultrashort x-ray pulses in real time. *Sci. Adv.* **2022**, *8*, abn6848.
(21) Yong, H.; et al. Observation of the molecular response to light upon photoexcitation. *Nat. Commun.* **2020**, *11*, 2157.
(22) Yang, J.; et al. Simultaneous observation of nuclear and electronic dynamics by ultrafast electron diffraction. *Science* **2020**, *368*, 885−889.
(23) Yong, H.; Cavaletto, S. M.; Mukamel, S. Ultrafast valence-electron dynamics in oxazole monitored by x-ray diffraction following a stimulated x-ray Raman excitation. *J. Phys. Chem. Lett.* **2021**, *12*, 9800−9806.
(24) Moreno Carrascosa, A.; et al. Mapping static core-holes and ring-currents with x-ray scattering. *Faraday Discuss.* **2021**, *228*, 60−81.
(25) Giri, S.; Tremblay, J. C.; Dixit, G. Imaging charge migration in chiral molecules using time-resolved x-ray diffraction. *Phys. Rev. A* **2021**, *104*, 053115.
(26) Bennett, K.; Kowalewski, M.; Rouxel, J. R.; Mukamel, S. Monitoring molecular nonadiabatic dynamics with femtosecond x-ray diffraction. *Proc. Natl. Acad. Sci. U.S.A.* **2018**, *115*, 6538−6547.
(27) Tegze, M.; Faigel, G. X-ray holography with atomic resolution. *Nature* **1996**, *380*, 49−51.
(28) Marchesini, S.; et al. Massively parallel x-ray holography. *Nat. Photonics* **2008**, *2*, 560−563.
(29) Feist, A.; et al. Ultrafast transmission electron microscopy using a laser-driven field emitter: Femtosecond resolution with a high coherence electron beam. *Ultramicroscopy* **2017**, *176*, 63−73.
(30) Rouxel, J. R.; Kowalewski, M.; Bennett, K.; Mukamel, S. X-Ray sum frequency generation; direct imaging of ultrafast electron dynamics. *Phys. Rev. Lett.* **2018**, *120*, 243902.
(31) Cho, D.; Rouxel, J. R.; Kowalewski, M.; Lee, J. Y.; Mukamel, S. Attosecond x-ray diffraction triggered by core or valence ionization of a dipeptide. *J. Chem. Theory Comput.* **2018**, *14*, 329−338.
(32) Woerner, M.; et al. Concerted electron and proton transfer in ionic crystals mapped by femtosecond x-ray powder diffraction. *J. Chem. Phys.* **2010**, *133*, 064509.
(33) Vrakking, M. J. J.; Elsaesser, T. X-rays inspire electron movies. *Nat. Photonics* **2012**, *6*, 645−647.
(34) Bennett, K.; Kowalewski, M.; Mukamel, S. Comment on "self-referenced coherent diffraction x-ray movie of angstrom- and femtosecond-scale atomic motion. *Phys. Rev. Lett.* **2017**, *119*, 069301.
(35) Ishikawa, T.; et al. Direct observation of collective modes coupled to molecular orbital-driven charge transfer. *Science* **2015**, *350*, 1501−1505.
(36) Li, Z.; Gyawali, S.; Ischenko, A. A.; Hayes, S.; Miller, R. J. D. Mapping atomic motions with electrons: Toward the quantum limit to imaging chemistry. *ACS Photonics* **2020**, *7*, 296−320.
(37) Zhang, M.; et al. Quantum state tomography of molecules by ultrafast diffraction. *Nat. Commun.* **2021**, *12*, 5441.
(38) Yong, H.; Keefer, D.; Mukamel, S. Imaging purely nuclear quantum dynamics in molecules by combined x-ray and electron diffraction. *J. Am. Chem. Soc.* **2022**, *144*, 7796−7804.
(39) Rouxel, J. R.; Keefer, D.; Mukamel, S. Signatures of electronic and nuclear coherences in ultrafast molecular x-ray and electron diffraction. *Struct. Dyn.* **2021**, *8*, 014101.
(40) Dixit, G.; Slowik, J. M.; Santra, R. Theory of time-resolved nonresonant x-ray scattering for imaging ultrafast coherent electron motion. *Phys. Rev. A* **2014**, *89*, 043409.

(41) Simmermacher, M.; Carrascosa, A. M.; Henriksen, N. E.; Møller, K. B.; Kirrander, A. Theory of ultrafast x-ray scattering by molecules in the gas phase. *J. Chem. Phys.* **2019**, *151*, 174302.
(42) Ma, L.; et al. Ultrafast x-ray and electron scattering of free molecules: a comparative evaluation. *Struct. Dyn.* **2020**, *7*, 034102.
(43) Huang, S.; et al. Generating single-spike hard x-ray pulses with nonlinear bunch compression in free-electron lasers. *Phys. Rev. Lett.* **2017**, *119*, 154801.
(44) Duris, J.; et al. Tunable isolated attosecond x-ray pulses with gigawatt peak power from a free-electron laser. *Nat. Photonics* **2020**, *14*, 30−36.
(45) Qi, F.; et al. Breaking 50 fs resolution barrier in MeV ultrafast electron diffraction with a double bend achromat compressor. *Phys. Rev. Lett.* **2020**, *124*, 134803.
(46) Li, C.; et al. Relativistic attosecond electron pulses from a photocathode radio-frequency gun. *Phys. Rev. Appl.* **2021**, *16*, 054007.
(47) Li, C.; et al. Fem-femtosecond MeV electron bunches for ultrafast electron diffraction. *Phys. Rev. Appl.* **2022**, *17*, 064012.
(48) Kirsch, P.; Hahn, A. Liquid crystals based on hypervalent sulfur fluorides: exploring the steric effects of ortho-fluorine substituents. *Eur. J. Org. Chem.* **2005**, *2005* (2005), 3095−3100.
(49) Jang, M.-S.; Song, S.-Y.; Shim, H.-K. Efficient green light-emitting polymer by balanced injection of electron and hole: new electron accepting perfluorinated substituent. *Polymer* **2000**, *41*, 5675−5679.
(50) Facchetti, A.; Yoon, M. H.; Stern, C. L.; Katz, H. E.; Marks, T. J. Building blocks for n-type organic electronics: regiochemically modulated inversion of majority carrier sign in perfluoroarene-modified polythiophene semiconductors. *Angew. Chem., Int. Ed.* **2003**, *42*, 3900−3903.
(51) Ostroverkhova, O. Organic optoelectronic materials: Mechanisms and applications. *Chem. Rev.* **2016**, *116*, 13279−13412.
(52) Campagnola, P. Second harmonic generation imaging microscopy: Applications to diseases diagnostics. *Anal. Chem.* **2011**, *83*, 3224−3231.
(53) Li, S.; et al. Attosecond coherent electron motion in Auger-Meitner decay. *Science* **2022**, *375*, 285−290.
(54) Kierspel, T.; et al. X-ray diffractive imaging of controlled gas-phase molecules: Toward imaging of dynamics in the molecular frame. *J. Chem. Phys.* **2020**, *152*, 084307.
(55) Ma, Z.; et al. Ultrafast isolated molecule imaging without crystallization. *Proc. Natl. Acad. Sci. U.S.A.* **2022**, *119*, e2122793119.
(56) Stankus, B.; et al. Advances in ultrafast gas-phase x-ray scattering. *J. Phys. B: At. Mol. Opt. Phys.* **2020**, *53*, 234004.
(57) Centurion, M.; Wolf, T. J. A.; Yang, J. Ultrafast imaging of molecules with electron diffraction. *Annu. Rev. Phys. Chem.* **2022**, *73*, 21−42.
(58) Teichmann, S. M.; Silva, F.; Cousin, S. L.; Hemmer, M.; Biegert, J. 0.5-keV soft x-ray attosecond continua. *Nat. Commun.* **2016**, *7*, 11493.
(59) Li, J.; et al. 53-attosecond x-ray pulses reach the carbon K-edge. *Nat. Commun.* **2017**, *8*, 186.
(60) Xue, B.; et al. A custom-tailored multi-TW optical electric field for gigawatt soft-x-ray isolated attosecond pulses. *Ultrafast Science* **2021**, *2021*, 9828026.
(61) Healion, D.; Zhang, Y.; Biggs, J. D.; Govind, N.; Mukamel, S. Entangled valence electron-hole dynamics revealed by stimulated attosecond x-ray Raman scattering. *J. Phys. Chem. Lett.* **2012**, *3*, 2326−2331.

https://doi.org/10.1021/jacs.2c07997
J. Am. Chem. Soc. 2022, 144, 20710−20716

Supporting Information:

Attosecond Charge Migration in Molecules Imaged by Combined X-Ray and Electron Diffraction

Haiwang Yong*, Shichao Sun, Bing Gu, Shaul Mukamel*

Department of Chemistry, University of California, Irvine, California 92697, United States

Department of Physics and Astronomy, University of California, Irvine, California 92697, United States

* Correspondence to: smukamel@uci.edu (S. M.) and h.yong@uci.edu (H. Y.)

Ab initio quantum chemistry

The molecular geometry was optimized using DFT with the B3LYP functional[1,2,3,4] and the 6-31g(d) basis set with Gaussian 16 software[5]. Core excited states were computed with TDDFT in the Tamm-Dancoff approximation (TDA) using the Chronus Quantum software package[6]. The TDA calculations employed the same density functional and basis set used in the geometry optimization. 22 lowest oxygen K-edge singlet excited states and 21 lowest fluorine K-edge singlet excited states were computed (excitation energies are shown in Table S1). The electronic charge densities and transition charge densities between core excited states i and j in real space were computed by contracting the atomic orbital basis with transition one particle density matrix (1pdm):

$$\sigma_{ij}^{\mathrm{E}}(\mathbf{r}) = \sum_{\mu\nu} D_{\mu\nu}^{ij} \chi_{\mu}(\mathbf{r}) \chi_{\nu}(\mathbf{r}) \tag{S1}$$

where $\mathbf{r}$ is the electronic coordinates, $\chi_{\mu}(\mathbf{r})$, $\chi_{\nu}(\mathbf{r})$ are atomic orbital basis, μ,ν are atomic orbital index and $D_{\mu\nu}^{ij}$ is transition 1pdm in atomic orbital basis. The grid-based $\sigma_{ij}^{\mathrm{E}}(\mathbf{r})$ in real space was calculated from the charge density matrices using PySCF software[7,8]. The electronic charge densities in $\mathbf{q}$-space (reciprocal space) were evaluated by

$$\sigma_{ij}^{\mathrm{E}}(\mathbf{q}) = \int \mathrm{d}\mathbf{r} e^{i\mathbf{q}\cdot\mathbf{r}} \sigma_{ij}^{\mathrm{E}}(\mathbf{r}) \tag{S2}$$

The nuclear charge density in $\mathbf{q}$-space for a given nuclear structure $\mathbf{R}$ was calculated as

$$\sigma^{\mathrm{N}}(\mathbf{q}, \mathbf{R}) = \sum_{a} Z_a e^{i\mathbf{q}\cdot\mathbf{R}_a(\mathbf{R})} \tag{S3}$$

where a labels the a_{th} atom with atomic number Z_a at position $\mathbf{R}_{\boldsymbol{a}}(\mathbf{R})$.

Table S1. Calculated excitation energies for core-excited states.

	Oxygen K-edge	Fluorine K-edge
1	520.311484337369	670.433707106402
2	520.692473844674	670.759254956266
3	521.176826061443	671.422828436184
4	521.499967962606	672.270655785232
5	522.028761263342	672.96904780278
6	523.364576338612	673.481471251711
7	523.976201403015	674.279712909104
8	524.594707207895	674.729513638568
9	524.919348161858	675.05881761288
10	525.383946792538	675.087887100853
11	525.449746918523	675.555327094097
12	526.009354804224	675.608487400162
13	526.127693551431	676.208811922601
14	526.150564177552	676.322894704176
15	526.285708774763	676.469374045217
16	526.509226087429	677.362492775789
17	527.18314732354	677.571509575662
18	527.767705930576	678.025021256983
19	528.348972026264	679.009046257872
20	529.201689395732	679.325787408199
21	529.645438483985	679.880050892203
22	529.958415684725	

Electron dynamics simulations

We adopt an attosecond Gaussian laser pulse to excite the core electrons in the molecule. The electric field is given by $\mathbf{E}(t) = \Re\left[\boldsymbol{\epsilon} E_0 e^{-(t-t_c)^2/\tau^2} e^{-i\omega_c(t-t_c)}\right]$ where τ is the pulse duration, ϵ the polarization, ω_c is the central frequency, and E_0 is the field amplitude. The laser-driven dynamics was simulated by solving the time-dependent Schrödinger equation in the presence of x-ray pulses, $i\hbar\left|\dot{\psi}(t)\right\rangle = (H_0 - \boldsymbol{\mu}\cdot\mathbf{E}(t))|\psi(t)\rangle$, with the fourth-order Runge-Kunta method. A linearly polarized x-ray pulse with its polarization direction parallel to the *x* direction was used. We use $\omega_c = 525$ eV for the oxygen K-edge, and 675 eV for the fluorine K-edge. For both simulations, the intensity $I = \frac{1}{2}c_0 E_0^2 = 6 \times 10^{13}$ W/cm^2, and FWHM in time is 365 attoseconds corresponding to a 5eV bandwidth. The laser-driven dynamics were performed from the initial time $t_i = -600$ as to the final time $t_f = 600$ as with a 0.2 as time step.

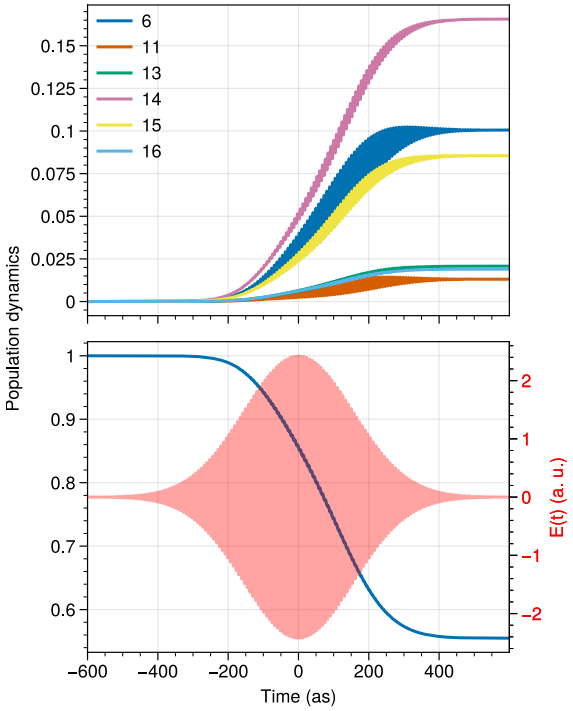

Figure S1. Population dynamics for the x-ray pump pulse tuned to the oxygen K-edge. (Upper) The excited state population dynamics, and (lower) the ground state population dynamics along with the electric field profile.

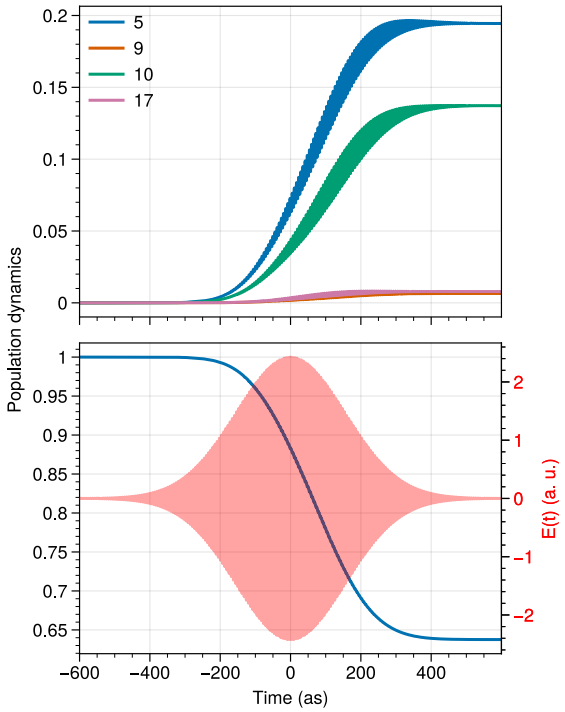

Figure S2. Same as Fig. S1 but for the x-ray pump pulse tuned to the fluorine K-edge.

Table S2. Key core-excited electronic states involved in the simulated electron dynamics and their molecular orbital excitation contributions (molecular orbitals are shown in Figure S3).

Oxygen K-edge		
Core-excited electronic states	Molecular orbital excitation contributions	Amplitudes
S6	2 -> 55	0.34508
	2 -> 56	0.59508
S14	2 -> 59	0.16916
	2 -> 61	-0.11738
	2 -> 62	-0.10059
	2 -> 63	-0.30328
	2 -> 64	0.33028
	2 -> 66	0.43545
	2 -> 68	-0.16405
S15	2 -> 62	0.47056
	2 -> 63	0.27993
	2 -> 64	-0.15321
	2 -> 66	0.37557
	2 -> 68	-0.11685
Fluorine K-edge		
S5	1 -> 55	0.60651
	1 -> 56	-0.22790
	1 -> 62	-0.18700
	1 -> 63	-0.10807
	1 -> 64	-0.10196
S10	1 -> 55	0.23433
	1 -> 56	-0.10110
	1 -> 58	0.12840
	1 -> 60	-0.10214
	1 -> 62	0.46651
	1 -> 63	0.24888
	1 -> 64	0.33756

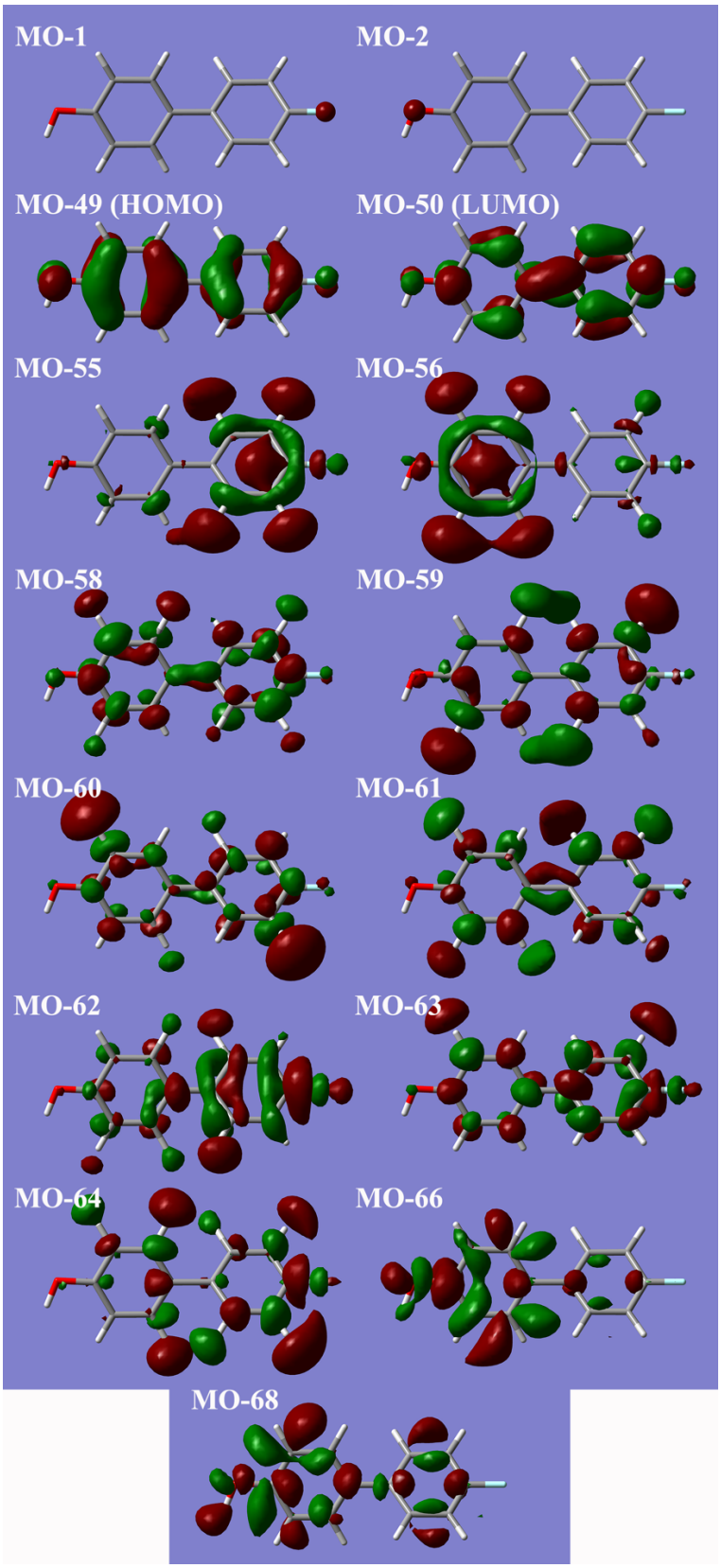

Figure S3. Molecular orbitals described in Table S2.

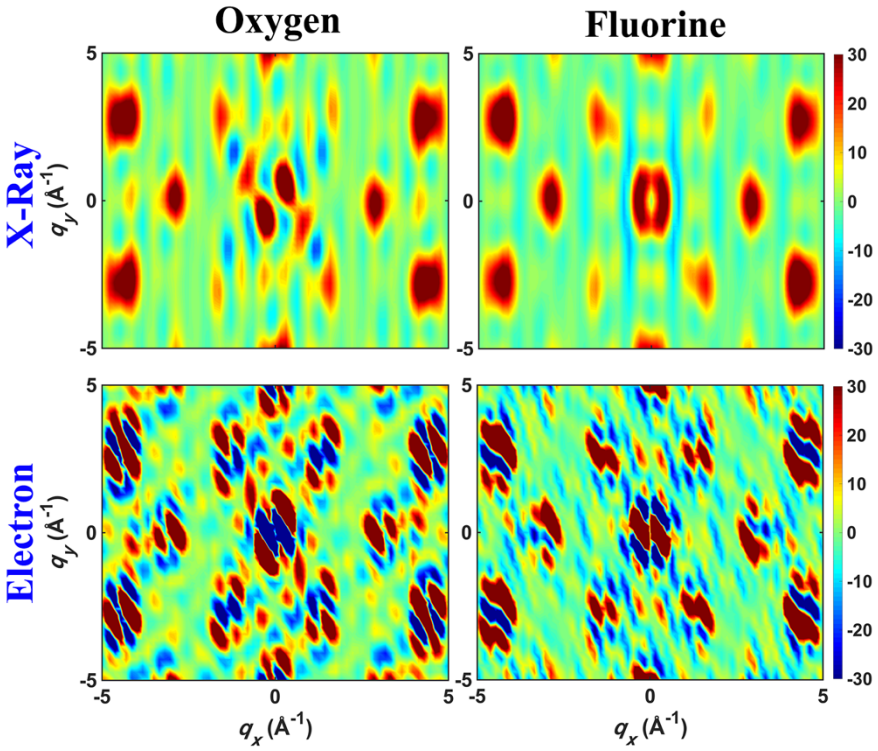

Figure S4. Time-dependent difference signals at 0.6 fs, $\Delta S_{\mathrm{XRD/UED}}(\mathbf{q}, t) = S_{\mathrm{XRD/UED}}(\mathbf{q}, t) - S_{\mathrm{XRD/UED}}(\mathbf{q}, t < 0)$, for x-ray (top) and electron (bottom) diffraction after excitation with x-ray pump pulse tuned to the oxygen (left) and fluorine (right) K-edges. The Cartesian coordinates are same as Figure 1 in main text. The signals are shown in the q_x-q_y plane (q_z = 0).

Supplementary references

1. Becke, A. D. Density-Functional Exchange-Energy Approximation with Correct Asymptotic Behavior. *Phys. Rev. A* **38**, 3098 (1988).
2. Becke, A. D. Density-Functional Thermochemistry. III. The Role of Exact Exchange. *J. Chem. Phys*. **98**, 5648 (1993).
3. Lee, C.; Yang, W.; Parr, R. G. Development of the Colle-Salvetti Correlation-Energy Formula into a Functional of the Electron Density. *Phys. Rev. B* **37**, 785 (1988).
4. Miehlich, B.; Savin, A.; Stoll, H.; Preuss, H. Results Obtained with the Correlation Energy Density Functionals of Becke and Lee, Yang and Parr. *Chem. Phys. Lett.* **157**, 200–206 (1989).
5. Frisch, M. J. et al. Gaussian 16 Revision A.03. Gaussian Inc. Wallingford CT (2016).
6. Williams-Young, D. B.; Petrone, A.; Sun, S.; Stetina, T. F.; Lestrange, P.; Hoyer, C. E.; Nascimento, D. R.; Koulias, L.; Wildman, A.; Kasper, J.; Goings, J. J.; Ding, F.; DePrince III, A. E.; Valeev, E. F.; Li, X. The Chronus Quantum Software Package. *Wiley Interdiscip. Rev. Comput. Mol. Sci.* e1436 (2019).
7. Sun, Q.; Berkelbach, T. C.; Blunt, N. S.; Booth, G. H.; Guo, S.; Li, Z.; Liu, J.; McClain, J.; Sharma, S.; Wouters, S.; et al. PySCF: the Python-Based Simulations of Chemistry Framework. *Wiley Interdiscip. Rev. Comput. Mol. Sci.* **2018**, *8*, e1340.
8. Sun, Q.; Zhang, X.; Banerjee, S.; Bao, P.; Barbry, M.; Blunt, N. S.; Bogdanov, N. A.; Booth, G. H.; Chen, J.; Cui, Z.-H.; et al. Recent Developments in the PySCF Program Package. *J. Chem. Phys.* **2020**, *153*, 024109.